ZANCO Journal of Pure and Applied Sciences
The official scientific journal of Salahaddin University-Erbil
https://zancojournals.su.edu.krd/index.php/JPAS

ISSN (print):2218-0230**, ISSN (online):** 2412-3986**, DOI: http://dx.doi.org/10.21271/zjpas**

RESEARCH PAPER

Urban Flood Simulation in Erbil City by Using Storm Water Management Model (SWMM)

Bakhtiyar A. Ali[1], Dana K. Mawlood[2]

[1]Department of Water Resources Engineering, College of Engineering, Salahaddin University-Erbil, Kurdistan Region, Iraq
[2]Department of Civil Engineering, College of Engineering, Salahaddin University- Erbil, Kurdistan Region, Iraq

A B S T R A C T:
One of the worst and most frequent natural disasters is flooding. Due to changes in precipitation patterns brought on by global climate change, flash floods are a threat to most cities. When it rains heavily, infrastructure capacity could be insufficient, and flash floods occur at weak points. This study evaluates the drainage system network capacity of the worst flood risk area using the Storm Water Management Model (SWMM). The study area is around the Council of Ministers, which is divided into 23 sub-catchments, and maximum daily rainfall data was collected from the Erbil Directorate of Meteorology and Seismology. This study analyzed three maximum daily rainfall events in three different decades of rainfall data from 1992–2022 to estimate the likelihood of flooding. The three events associated with maximum daily precipitation were 103.9 mm, 79.0 mm, and 71.8 mm on February 3, 2006, November 21, 1992, and January 28, 2013, respectively, using the Indian Meteorological Department (IMD) method to convert daily rainfall data to hourly rainfall. The dynamic wave routing method is used for flow routing, and the Horton equation is used to measure infiltration. The flood rate amount in the nodes is classified into three stages: moderate flood (0.001 - 0.1 m^3/s), high flood (0.1 - 0.5 m^3/s), and very high flood (more than 0.5 m^3/s). The results showed that the number of flood nodes is (14, 10, and 10) for each of the three events, with (4, 3, and 3) nodes experiencing moderate floods, (5, 6, and 6) nodes experiencing high flood rates, and (5, 1, and 1) nodes experiencing very high flood rates. It is indicated that the drainage system networks in the study area are unable to handle the amount of runoff and are poorly constructed.

KEY WORDS: Urban flooding; SWMM; Dynamic wave method; Horton equation
DOI: http://dx.doi.org/10.21271/ZJPAS.35.5.1
ZJPAS (2023) , 35(5);1-11 .

1.INTRODUCTION:

Flooding is a common, wide-ranging, and frequent natural hazard that causes significant socioeconomic and environmental damage around the world (Barredo, 2009, Teng et al., 2017). Flood risk is especially high in urban areas with varying land surfaces, and human activity causes significant changes in hydrological processes (Guan et al., 2015, Sillanpää and Koivusalo, 2015). In general, intense rainfalls cause urban surface water flooding when the capacity of urban drainage systems is insufficient (Falconer et al., 2009, Chen et al., 2015).

The recent floods in Erbil's downtown area have enhanced public awareness about the dangers of urban flooding. The urbanization of a watershed can have a significant impact on runoff discharge, and the hydrograph.

As a result of urbanization, permeable surfaces are being replaced with impermeable surfaces, such as streets, parking lots, and buildings. In recent years, big metropolitan centers such as Erbil have seen numerous urban flood situations. Due to a lack of proper drainage infrastructure and climate change variables, high-intensity rainfall events that are unexpected in nature are becoming a serious challenge in urban catchments.

* **Corresponding Author:**
Bakhtiyar Ahmed Ali
E-mail: bakhtiyar.ali@su.edu.krd or baxtiyar2010@gmail.com
Article History:
Received: 10/09/2022
Accepted: 29/01/2023
Published: 25/10 /2023

SWMM can be used to design drainage systems and to simulate dynamic single-event and continuous events in pipes, channels, storage or treatment devices, pumps, and outlets that are commonly used to divert runoff. Flood modeling is primarily used to investigate all aspects of flooding in the urban environment, including the effects of heavy rainfall on the runoff of urban sub-catchments and the many socio-economic aspects of flooding.

Unfortunately, as a result of this recent flood, a number of people lost their lives, the streets were severely damaged, many people were financially damaged, and their houses and cars were damaged. The KRG should therefore consider a comprehensive and strategic plan for the future. In this aspect, several studies have been conducted on flooding in urban areas, such as:

In the Erbil sub-basin of the Kurdistan Region of Iraq, (Hameed, 2017) investigated a study to analyse the impact of urban expansion and other changes in land use on runoff response over the study period of 1984 to 2014. The findings show that between 1984 and 2004 and between 2004 and 2014, the urbanization of the watershed increased the amount of impervious land cover by 71% and 51%, respectively. Urban expansion is to blame for the increase in impervious surface area, which led to an 85% increase in runoff volume between 1984 and 2014. The study also makes the point that when estimating surface runoff, the watershed's slope in the Erbil sub-basin should be taken into account because the area upstream has a steep gradient and little to no vegetation, which enhances the flow's velocity and raises the risk of flooding in Erbil City.

(Gharib et al., 2021) investigated a study to estimate how much rainwater was collected from the Sulaimani Heights urban area in Sulaimani City. Using daily rainfall data from 1991 to 2019, the stormwater management model (SWMM), the soil conservation service (SCS) method, and the runoff coefficient (RC) method have been compared. According to the three separate methodologies (SWMM, SCS, and RC), the yearly harvested runoff results were predicted to be 836,470 m3, 508,454 m3, and 737,381 m3, respectively. Compared to the RC and SCS methods, which had runoff results of 28% and 19%, respectively, the SWMM method had the highest runoff result and could meet 31% of the study area's total demand.

Many researchers around the world have tried to model floods in urban and rural areas using geospatial methodologies (Abdelkarim et al., 2019, Bouaida et al., 2021) (Desalegn and Mulu, 2021, Hermas et al., 2021) (Mohamed, 2019, Portugués-Mollá et al., 2016) (Samela et al., 2018) for evaluating rainfall (Courty et al., 2018, Notaro et al., 2013) (Rahmani et al., 2016), and finally, a mapping and analysis of flood risk (Cabrera and Lee, 2020) (Oubennaceur et al., 2019).

2. MATERIALS AND METHODS

2.1. Storm Water Management Model (SWMM)

The Storm Water Management Model (SWMM) of the United States Environmental Protection Agency (US-EPA) is a dynamic rainfall-runoff simulation model that can be used for single-event or long-term (continuous) simulation of runoff quantity and quality from mostly urban areas. SWMM's runoff component works on a collection of sub-catchment regions that receive precipitation and produce runoff and pollutant loads. SWMM's routing module distributes the runoff through a network of pipelines, channels, storage and treatment devices, pumps, and regulators. During a simulation period made up of numerous time steps, SWMM tracks the quantity and quality of runoff generated inside each sub-catchment, as well as the flow rate, flow depth, and quality of water in each pipe and channel. SWMM was created in 1971 and is still in use today. It is still widely used around the world for the planning, analysis, and design of stormwater runoff, combined sewers, sanitary sewers, and other drainage systems in urban areas, with numerous non-urban uses as well. Version 5 is a total rewrite of the preceding edition. SWMM 5 is a Windows-based program that allows you to edit study area data, conduct hydrologic, hydraulic, and water quality simulations, and examine the results in a variety of formats (Rossman, 2010)

2.2 Study Area

Erbil is the capital of the Kurdistan Region. Erbil Province covers a total area of 14,873.68 km^2, although the study area is the city core and urbanized area as shown in Fig. 1a. It is located at 36° 11' 55.58" and 36° 11' 14.74" latitude and 44° 0' 58.15" and 43° 59' 28.76" longitude, with an average node bottom invert elevation of 400-393.38 m above sea level, with the study area extending from Tairawa quarter to the Council of Ministers, which is prone to flooding during the rainy season.

Fig.1a: Satellite Image of Erbil City

2.3 Topography

Erbil is a flat, hilly region with flat plains in the west and southwest and hills in the north and northeast. Erbil's central plain gently slopes east to west, with a slope of less than 3° and local slopes of less than 8° (Hassan, 1998). The elevation of the city center of Erbil district is between 440 m above sea level in the northeast and about 390 m above sea level in the southwest of the city, as shown in Fig.1b. The elevation of the study area is between 390 and 410 m above sea level.

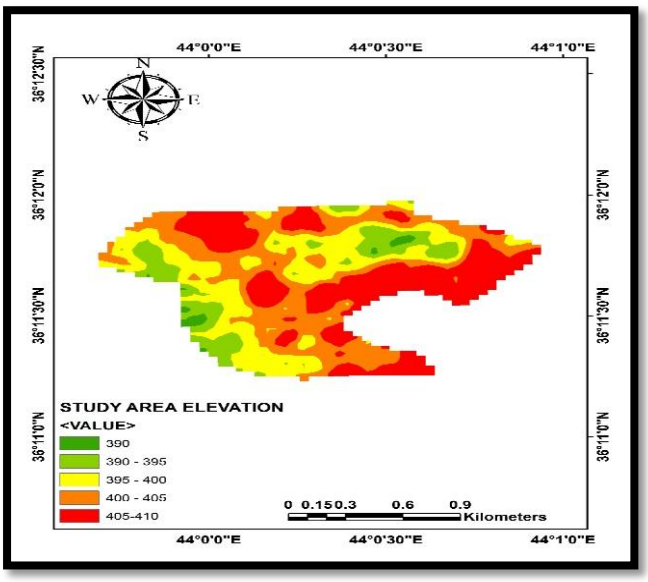

Fig.1b: Elevation of Central Erbil City

2.4 Climate Data

The climate of the Kurdistan Region of Iraq is defined by a chilly, rainy winter and a dry, warm summer. Throughout the winter, rainfall is brought in by cyclonic disruptions from the Mediterranean Sea as well as circulation around an anticyclone located over the Arabian Peninsula (Hama et al., 2014). The semiarid climate of Erbil has low summertime humidity and moderate wintertime humidity. The typical temperature varies between 6 and 16 degrees Celsius in the winter and between 25 and 40 degrees Celsius in the summer. Precipitation occurs most frequently between October and May each year. Jan and Dec are the months with the most rainfall (Mustafa et al., 2019). The long-term annual rainfall average is more than 400 mm. The rainy season typically begins in mid-October and continues until late May. The coldest months are December and January, while the hottest months are July and August.

2.5 Data Collection

All data used in this study were obtained from the Erbil Water and Sewerage Directorate, which includes the underground drainage network of the study area, consisting of manhole locations, elevations, underground sewerage concrete conduit lengths, and concrete pipes. The underground sewerage network is made up of three main networks, one of which is a closed, rectangular channel measuring 2*2 m that runs from the middle of the Tairawa quarter to the front

of the Council of Ministers. Another one begins near 60 Street and ends near 30 Street, near the Council of Ministers, and is a closed rectangular channel of 2*2 m that is over 800 m long, as shown in Fig.1c. All these canals and sewerage networks bring and collect water near the Council of Ministers, which is the lowest area compared with the surrounding area. And two concrete sewer pipes are usually located in the main streets, which are 1000 mm and 1250 mm in diameter, but it's recommended that about 30 cm of the sewer pipes be filled by sediment and many other things, such as wood, stones, bottles, and garbage.

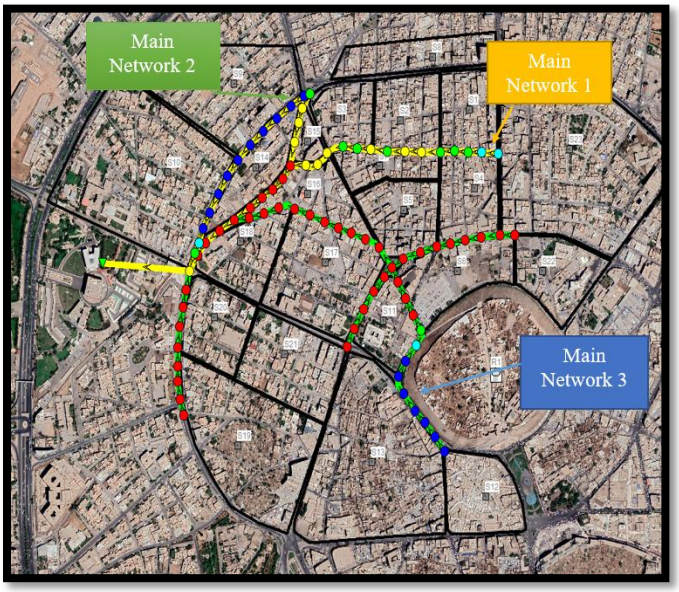

Fig.1c: Location of Main Networks and Sub-catchments

2.6 Model Setup

The research area's sub-catchment discretization in SWMM is accomplished by importing multiple drainage pathways and outlets from Google Earth Pro. The area is divided into 23 sub-catchments to create a schematic depiction of the area. The information for all sub-catchments is shown in Table 1. The runoff from these sub-catchments is collected in 84 nodes connected by 84 conduits and discharged at a single outfall, O1, as shown in Figure 2. In the model, properties such as invert level, depth, slope, size, and percentage of imperviousness are set for each sub-catchment. Similarly, each sub-catchment percent slope is defined using a slope map created using digital elevation model (DEM) data, as shown in Fig.3a. To calculate the percentage of impervious area of the sub-catchments, first download the digital elevation model (DEM) of the study area and then use ArcGIS 10.8 to determine the percentage of impervious area through the land use land cover map of the study area, as shown in Fig. 3b. The model is run on hourly time steps using historical extreme rainfall events. Horton's equation is utilized to compute infiltration in the model, while the dynamic wave method is employed for flow routing. The information about nodes and junctions, such as the bottom elevation and maximum depth of nodes, is given in Table 2.

Table (1): Sub-catchment Data

Sub catchment ID	Area (ha)	Width (m)	Ave slope (%)	Impervious area (%)
S1	3.55	169	2.2	90
S2	3.73	198	1.15	90
S3	2.79	133	0.5	88
S4	3.79	178	1.9	86
S5	3.79	172	0.5	90
S6	4.47	172	0.5	70
S7	2.35	97	1.6	90
S8	2.87	104	1.23	89
S9	8.72	305	0.5	87
S10	14.47	333	0.5	75
S11	2.69	113	3.5	70
S12	4.35	159	0.5	25
S13	14.32	293	1.0	80
S14	3.13	100	1.0	75
S15	0.74	71	0.5	90
S16	2.87	151	1.0	90
S17	7.25	290	1.0	70
S18	3.44	131	1.0	75
S19	10.82	278	2.0	60
S20	3.8	175	1.0	85
S21	5.58	175	1.0	85
S22	3.44	146	2.0	60
S23	17.3	344	2.0	80

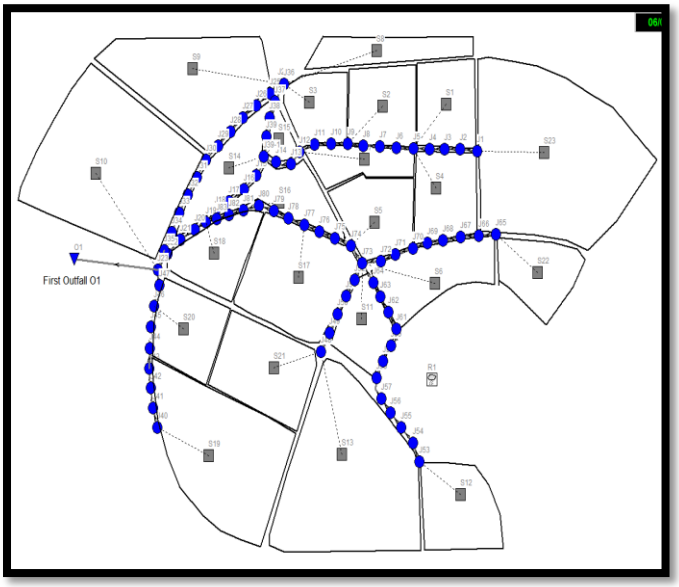

Fig.2: Sub-catchment Discretization

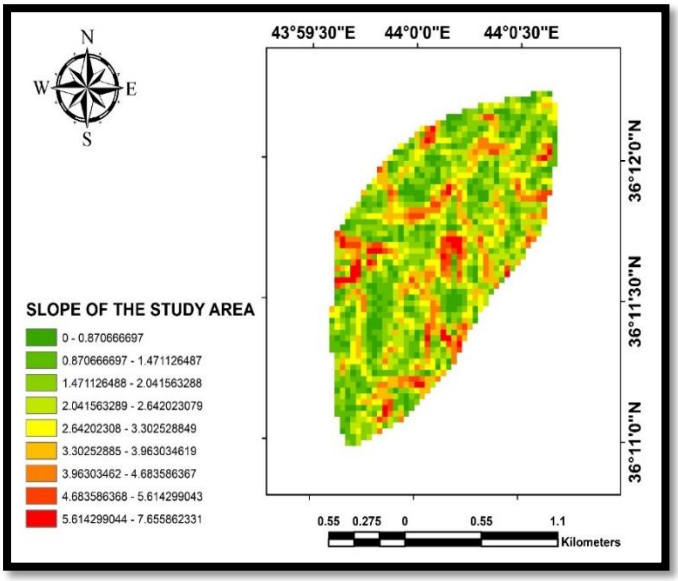

Fig.3a: Slope of The Study Area

Table (2): Information of Nodes

Node	Bottom elevation (m)	Max depth (m)	Node	Bottom elevation (m)	Max depth (m)	Node	Bottom elevation (m)	Max depth (m)
J1	398.01	3.21	J31	394.34	3.20	J60	398.24	1.5
J2	397.92	3.19	J32	394.2	3.15	J61	398.0	1.5
J3	397.73	3.30	J33	394.05	3.13	J62	397.75	1.5
J4	397.52	3.12	J34	393.75	3.16	J63	397.5	1.5
J5	397.41	3.15	J35	393.5	3.09	J64	397.3	1.5
J6	397.25	3.17	J36	395.5	3.11	J65	398	1.5
J7	397.04	3.40	J37	395.4	3.14	J66	397.9	1.5
J8	396.91	3.42	J38	395.3	3.2	J67	397.75	1.5
J9	396.75	3.43	J39	395.2	3.22	J68	397.6	1.5
J10	396.52	3.45	J39-1	395.1	3.20	J69	397.5	1.5
J11	396.32	3.40	J40	395.0	1.5	J70	397.35	1.5
J12	396.09	3.38	J41	394.7	1.5	J71	397.25	1.5
J13	395.73	3.35	J42	394.5	1.5	J72	397.1	1.5
J14	395.51	3.50	J43	394.3	1.5	J73	397.0	2.0
J15	394.90	3.44	J44	394.1	1.5	J74	396.7	2.0
J16	394.75	3.42	J45	393.9	1.5	J75	396.4	2.0
J17	394.57	3.40	J46	393.7	1.5	J76	396.1	2.0
J18	394.29	3.38	J47	393.5	1.5	J77	395.8	2.0
J19	393.90	3.30	J48	397.5	1.5	J78	395.5	2.0
J20	393.78	3.15	J49	397.4	1.5	J79	395.2	2.0
J21	393.62	3.10	J50	397.3	1.5	J80	394.9	2.0
J22	393.55	3.05	J51	397.2	1.5	J81	394.6	2.0
J23	393.38	3.00	J52	397.1	1.5	J82	394.3	2.0
J24	395.50	3.10	J53	400	1.5	J83	394.1	2.0
J25	395.35	3.12	J54	399.75	1.5	O1	392.5	2.0
J26	395.20	3.15	J55	399.5	1.5			
J27	395.00	3.16	J56	399.25	1.5			
J28	394.85	3.11	J57	399.0	1.5			
J29	394.70	3.19	J58	398.75	1.5			
J30	394.56	3.18	J59	398.5	1.5			

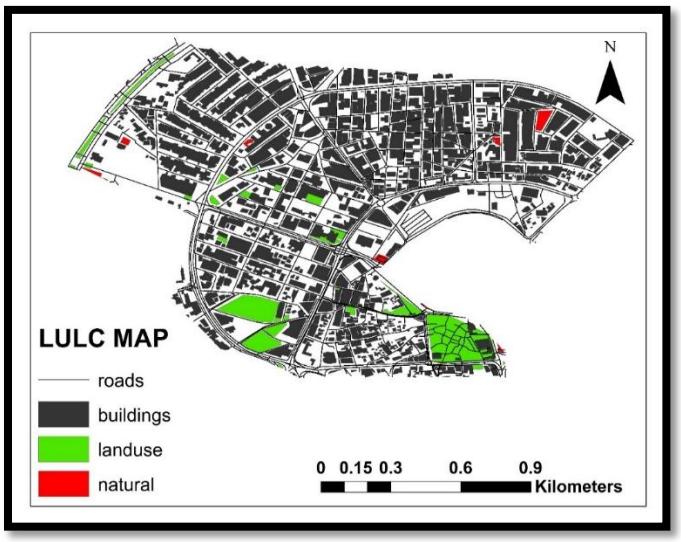

Fig. 3b: LULC Map of the Study Area

2.7. Dynamic Wave Routing Method

Dynamic wave routing produces the most theoretically precise results. Since it fully solves one-dimensional Saint Venant's flow equations. These equations include a volume continuity equation at nodes as well as continuity and momentum equations for conduits. With this type of routing, a pressured flow can pass the amount of full flow, and the Manning equation can be represented when a closed conduit fills to capacity. Flooding happens when the depth of water at a node exceeds the maximum depth that may be accommodated, and the extra flow either escapes from the system or can collect on top of the node and re-enter the drainage system. Channel storage, backwater, entrance/exit losses, flow reversal, and pressured flow can all be taken into consideration via dynamic wave routing. Any general network structure, including ones with several downstream diversions and loops, can use it since it combines the result for both water levels at nodes and flow in conduits. It is the preferred option for systems that experience severe backwater effects as a result of downstream flow limitations, with flow regulation provided by weirs and orifices. SWMM will automatically change the maximum time step set by the user as needed to keep the numbers stable. However, this flexibility comes at the cost of using much smaller time steps, on the order of a minute or less.

2.8. Infiltration Rate

This method is based on actual data demonstrating that, over the course of a prolonged rainfall event, infiltration of water declines exponentially from an initial maximum rate to some minimum rate. This method needs to know the maximum and minimum infiltration rates, how quickly the rate drops over time, and how long it takes for dry soil to become fully saturated.

$$fp = f\infty + (fo + f\infty)\, e^{-kdt} \quad \text{..... Eq (1)}$$

Where:

fp = infiltration capacity into soil (L/T)
$f\infty$ = minimum or equilibrium value of fp (at t = ∞) (L/T)
fo = maximum or initial value of fp (at t = 0) (L/T)
t = time from beginning of storm (T)
$k_{d=}$ decay coefficient (T^{-1})

3. RESULTS AND DISCUSSION

3.1. Flood Nodes for Three Events

After running the model with 103.9 mm of rain depth in the study area, generally, 14 nodes were flooded, accounting for 16.6 percent of the 84 nodes, with flooding amounts ranging from 0.007 m^3/s at node J76 to 0.906 m^3/s at node J74. The reason for the high flooding at node J74 is that the majority of the runoff water from the sub-catchment numbers (S5, S6, S11, S13, and S21) flows to this node, which has an area of around 28 hectares. The flood rate amount in the nodes is classified into three stages: from (0.001 – 0.1 m^3/s) moderate flooding, (0.1 – 0.5 m^3/s) high flooding, and more than 0.5 m^3/s very high flooding. The flood rate is moderate, with the first stage flood rate ranging from 0.007 to 0.092 m^3/s, and four nodes are inundated with moderate flooding at J76, J75, J62, and J41. Four nodes are inundated with high flood rates between (0.103–0.336 m^3/s), and the number of flood nodes in the second stage is five nodes: J80, J44, J46, J40, and J72. For the last stage, in which the amount of flood rate at the nodes is between (0.612 and 0.906 m^3/s), the number of flooded nodes is five nodes, with a very high flood rate consisting of nodes J73, J77, J83, J48, and J74. The location of the flooding node is shown in Fig.4a.

However, after running the model for the second event with 79 mm of rain depth in the

study area, the number of flooded nodes was reduced to 10 nodes, or 11.3% of all nodes in the study area, and the amount of flooding was greatly reduced so that the minimum flood amount was at node J80, which was only 0.007 m^3/s, as opposed to the minimum flood amount at node J75 in the first event. Furthermore, whereas in the first event the maximum flood rate was at node J74 with 0.906 m^3/s, in this event the maximum flood volume at node J74 decreased to 0.781 m^3/s. In this case, flood rates can be divided into three stages, with a moderate flood with a low risk to the study area falling between 0.007 and 0.065 m^3/s and only three nodes, J80, J46, and J41, as flood nodes. High floods also occur in nodes with flow rates ranging from 0.135 to 0.458 m^3/s, the number of flood nodes in this stage is six, which include J44, J72, J48, J73, J83, and J77.

For the third stage, with a flood rate greater than 0.5 m^3/s only one node J77 with a maximum rate of 0.781 m^3/s flooded. Fig.4b shows the location of the nodes where the flooding occurred. Ten nodes are flooded in the third event, where the rain depth was 71.8 mm, and the results are approximately similar to the second event with a little bit of difference. The study area is subject to considerable economic and human risks due to the flood. The average amounts of flooding for the first, second, and third scenarios are 0.367, 0.255, and 0.255 m^3/s respectively; all flooding node locations and data are illustrated in Fig.4c, and Table 3.

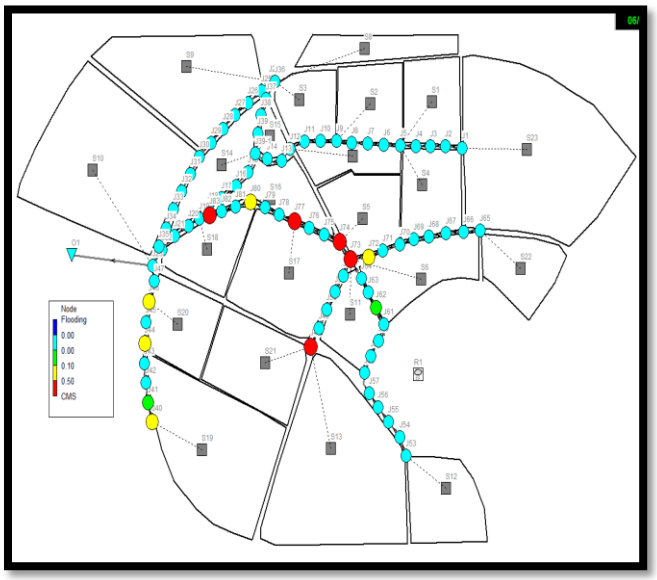

Fig.4a: Flood Nodes Location of 103.9 mm Rain Depth

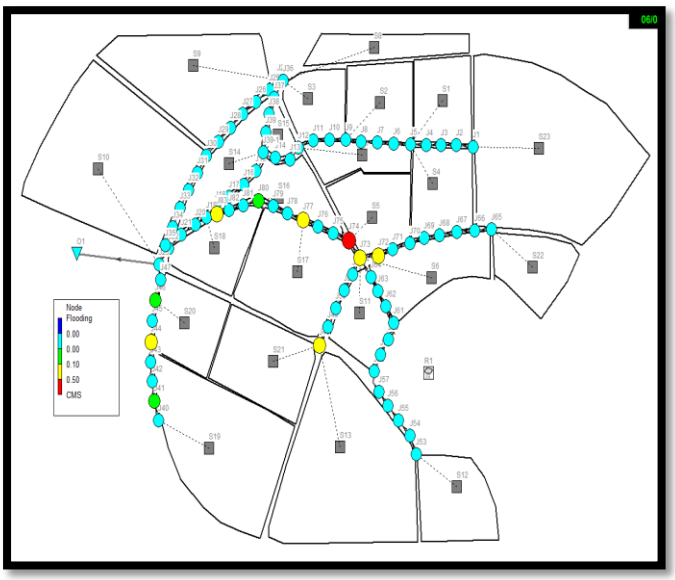

Fig.4b: Flood Nodes Location of 79 mm Rain Depth

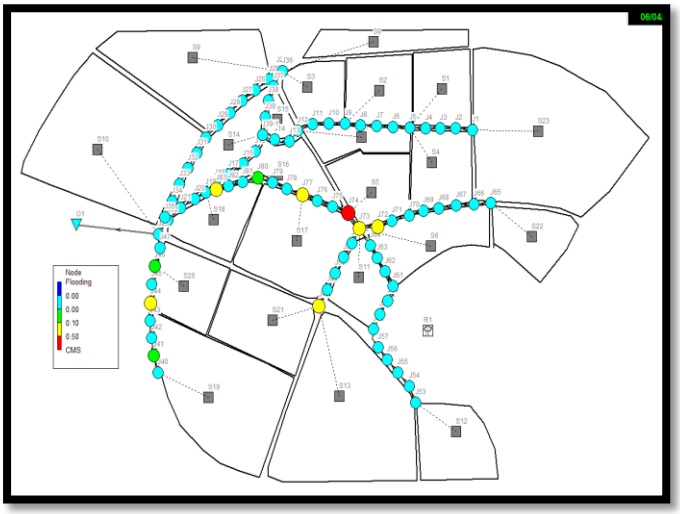

Fig.4c: Flood Nodes Location of 71.8 mm Rain Depth

Table (3): Flood Nodes

Node	Maximum rate of flood m^3/s	Node	Maximum rate of flood m^3/s
First Event		**Second Event**	
J76	0.007	J80	0.007
J75	0.023	J46	0.032
J62	0.027	J41	0.065
J41	0.092	J44	0.135
J80	0.103	J72	0.222
J44	0.135	J48	0.233
J46	0.158	J73	0.294
J40	0.327	J83	0.322
J72	0.336	J77	0.458
J73	0.612	J74	0.781
J77	0.699		
J83	0.758		
J48	0.884		

J74	0.906	
Average rate of flood m^3/s	0.363	0.255

3.2 Capacity of Links for Each Rain Depth Event

3.2.1 First Rainfall Event

The rain depth in the first event is 103.9 mm, the simulation's level of accuracy is best, and the continuity errors for surface runoff and flow routing are, respectively, -0.01 % and 0.07 %. In this event, 34 concrete circular pipes are depicted because the size of the pipes cannot accommodate runoff flow due to the inadequate diameter of the pipes. The maximum flow in link C78 is 1.454 m^3/s.

3.2.2 Second Rainfall Event

In the second scenario, the rain depth is 79 mm, the simulation accuracy is at its highest level, and the continuity errors for surface runoff and flow routing are, respectively, -0.01 % and 0.08 %. Due to the insufficient size of the pipes, this event depicts a setup of 29 links that cannot handle runoff flow, and the maximum flow through link C88 is 1.282 m^3/s.

3.2.3 Third Rainfall Event

In this scenario, the rain depth is 71.8 mm, the modeling accuracy is at its highest level, and the continuity errors for the flow routing and surface runoff are zero and 0.09 %, respectively. The results showed that 29 links cannot handle runoff flow due to the insufficient diameter of the pipes. The maximum flow at link C85 is 1.281 m^3/s. All of the links' maximum flows and depths are illustrated in Table 4.

Table (4): Maximum Flow and Depth of Links

Links	Max. flow m^3/s	Depth (m)	Links	Max. flow m^3/s	Depth (m)	Links	Max. flow m^3/s	Depth (m)
First event 103.9 mm rain depth			**Second event 79 mm rain depth**			**Third event 71.8 mm rain depth**		
C40	0.745	1.00	C40	0.718	0.97	C40	0.718	0.97
C41	0.653	0.96	C41	0.653	0.96	C41	0.653	0.96
C42	0.653	0.90	C42	0.653	0.89	C42	0.653	0.90
C43	0.653	0.93	C43	0.653	0.93	C43	0.653	0.93
C44	0.546	1.00	C44	0.543	1.00	C44	0.546	1.00
C45	0.547	1.00	C45	0.544	1.00	C45	0.548	1.00
C46	0.739	0.90	C46	0.739	0.90	C46	0.739	0.90
C47	0.739	0.73	C47	0.739	0.73	C47	0.739	0.73
C48	1.123	1.00	C48	1.111	1.00	C48	1.111	1.00
C49	1.108	0.99	C49	1.101	0.99	C49	1.101	0.99
C50	1.097	0.99	C50	1.094	0.98	C50	1.094	0.98
C51	1.091	0.99	C51	1.091	0.99	C51	1.091	0.99
C52	1.097	1.00	C52	1.091	1.00	C52	1.091	1.00
C61	0.432	0.66						
C62	0.405	0.72	C62	0.297	0.63			
C63	0.405	0.67				C63	0.352	0.63
C64	0.405	0.99	C64	0.322	1.00	C64	0.322	0.64
C71	0.340	0.85	C71	0.227	0.84	C71	0.227	0.85
C72	0.196	1.00	C72	0.197	1.00	C72	0.229	1.00
C73	**1.646**	**1.00**	**C73**	**1.640**	**1.00**	**C73**	**1.640**	**1.00**
C74	1.097	1.00	C74	1.080	1.00	C74	1.076	1.00
C75	1.071	1.00	C75	1.071	1.00	C75	1.070	0.99
C76	1.070	1.00	C76	1.70	1.00	C76	1.070	1.00
C77	1.181	0.99	C77	1.185	0.99	C77	1.179	0.99
C78	1.179	0.99	C78	1.184	0.99	C78	1.179	0.99
C79	1.179	0.99	C79	1.184	0.99	C79	1.074	0.99
C80	1.285	0.94	C80	1.282	0.94	C80	1.282	0.94
C81	1.285	0.84	C81	1.282	0.84	C81	1.281	0.84
C82	1.284	0.90	C82	1.281	0.90	C82	1.280	0.90

C83	1.284	1.00	C83	1.281	0.96	C83	1.280	0.96
C40	0.745	1.00	C40	0.718	0.97	C40	0.718	0.97
C41	0.653	0.96	C41	0.653	0.96	C41	0.653	0.96
C42	0.653	0.90	C42	0.653	0.89	C42	0.653	0.90

3.3Node J23 Total Inflow Hydrograph

The research area has been divided into 23 distinct sub-catchments with sewer lines and includes conduits and connections with the appropriate slope. Figs. 5a, 5b, and 5c each depict the runoff produced by the main sub-catchments of the study area for the three different rainfall scenarios. Because node J23 is in a high-risk location in the research area, the hydrographs help us understand the interaction between rainfall runoff and total inflow into junction 23. Between the start of the rain and 24 hours later, the maximum junctional total inflow was observed.

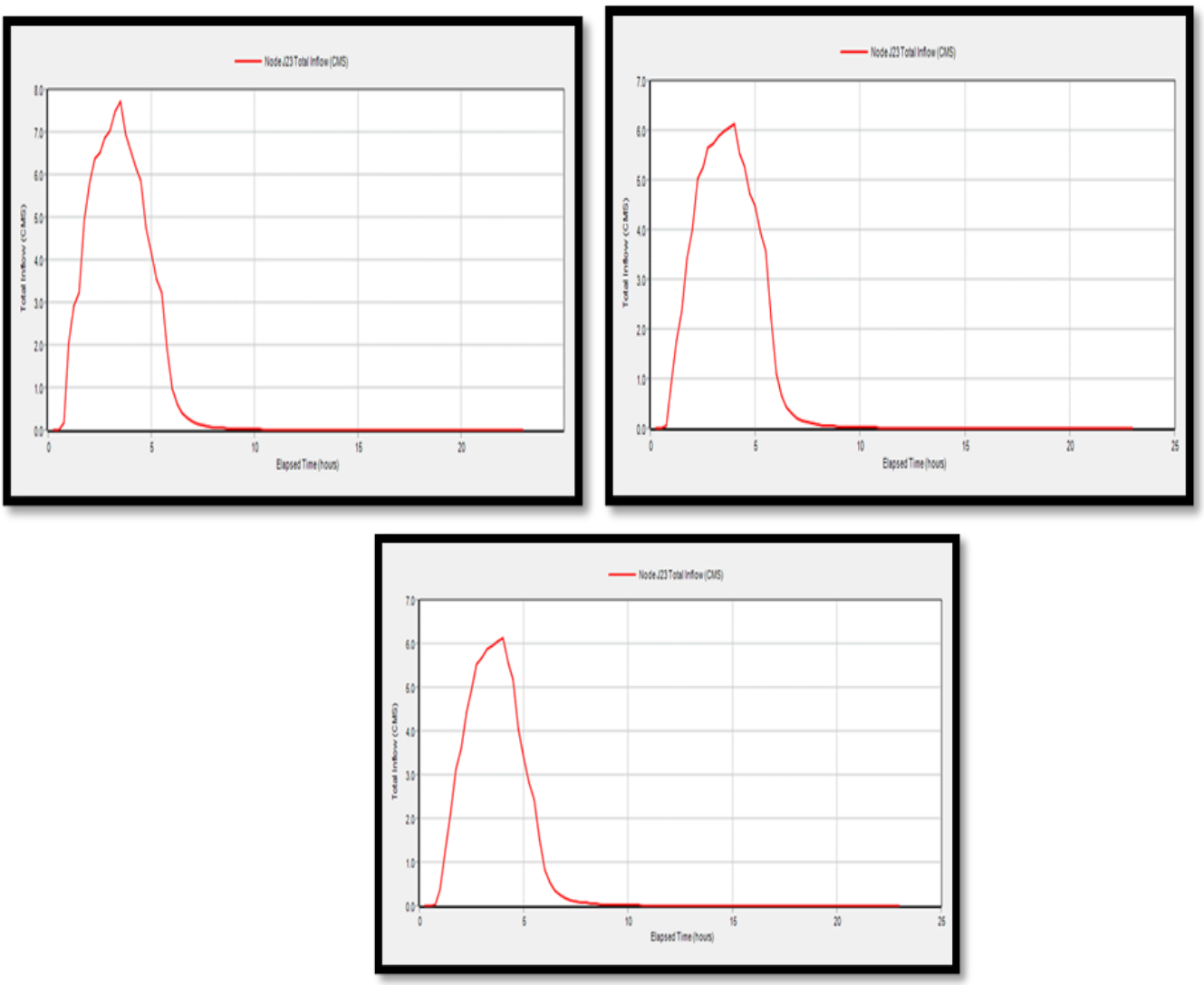

Fig. 5a, 5b, and 5c: Total Inflow Hydrograph of Node J23 for (103.9, 79, and 71.8) mm Rain depth

4. CONCLUSIONS

The current work simulates urban floods using the SWMM model. The Erbil Water and Sewerage Directorate provides the data needed to create the model. This model shows that SWMM is utilized for closed box channels and circular pipe flow. The result is based on three different maximum daily rainfall events converted to hourly that occurred on February 3, 2006, November 21, 1992, and January 28, 2013, respectively. The maximum daily precipitation for these three events was 103.9 mm, 79 mm, and 71.8 mm. According to the simulation results for the first event, the nodes J76, J75, J62, J41, J80, J44, J46, J40, J72, J73, J77, J83, J48, and J74 experienced the highest levels of flooding. Maximum flooding occurred at nodes J80, J46, J41, J44, J72, J48, J73, J83, J77, and J74 for the second and third events, respectively.

References

ABDELKARIM, A., GABER, A. F., YOUSSEF, A. M. & PRADHAN, B. 2019. Flood hazard assessment of the urban area of Tabuk City, Kingdom of Saudi Arabia by integrating spatial-based hydrologic and hydrodynamic modeling. *Sensors,* 19**,** 1024.

BARREDO, J. I. 2009. Normalised flood losses in Europe: 1970–2006. *Natural hazards and earth system sciences,* 9**,** 97-104.

BOUAIDA, J., WITAM, O., IBNOUSSINA, M., DELMAKI, A. E. F. & BENKIRANE, M. 2021. Contribution of remote sensing and GIS to analysis of the risk of flooding in the Zat basin (High Atlas-Morocco). *Natural Hazards,* 108**,** 1835-1851.

CABRERA, J. S. & LEE, H. S. 2020. Flood risk assessment for Davao Oriental in the Philippines using geographic information system- based multi-criteria analysis and the maximum entropy model. *Journal of Flood Risk Management,* 13**,** e12607.

CHEN, Y., ZHOU, H., ZHANG, H., DU, G. & ZHOU, J. 2015. Urban flood risk warning under rapid urbanization. *Environmental research,* 139**,** 3-10.

COURTY, L. G., RICO-RAMIREZ, M. Á. & PEDROZO-ACUÑA, A. 2018. The significance of the spatial variability of rainfall on the numerical simulation of urban floods. *Water,* 10**,** 207.

DESALEGN, H. & MULU, A. 2021. Mapping flood inundation areas using GIS and HEC-RAS model at Fetam River, Upper Abbay Basin, Ethiopia. *Scientific African,* 12**,** e00834.

FALCONER, R. H., COBBY, D., SMYTH, P., ASTLE, G., DENT, J. & GOLDING, B. 2009. Pluvial flooding: new approaches in flood warning, mapping and risk management. *Journal of Flood Risk Management,* 2**,** 198-208.

GHARIB, K. N., MUSTAFA, N. F. & RASHID, H. M. 2021. Urban Rainwater Harvesting Assessment in Sulaimani Heights District, Sulaimani City, KRG, Iraq. *UHD Journal of Science and Technology,* 5**,** 48-55.

GUAN, M., SILLANPÄÄ, N. & KOIVUSALO, H. 2015. Modelling and assessment of hydrological changes in a developing urban catchment. *Hydrological Processes,* 29**,** 2880-2894.

HAMA, R. H., HAMAD, R. T. & AZIZ, F. H. 2014. Climate change in relation to rainfall and temperature in Erbil province, Kurdistan, Iraq. *Tunisian Association of Digital Geographic Information, 8Th International Congers Geo Tunis, Tunis,* 8.

HAMEED, H. M. 2017. Estimating the effect of urban growth on annual runoff volume using GIS in the Erbil sub-basin of the Kurdistan Region of Iraq. *Hydrology,* 4**,** 12.

HASSAN, I. 1998. Urban hydrology of Erbil city Region. *Degree of doctor of philosophy in geology (hydrogeology). University of Baghdad*.

HERMAS, E., GABER, A. & EL BASTAWESY, M. 2021. Application of remote sensing and GIS for assessing and proposing mitigation measures in flood-affected urban areas, Egypt. *The Egyptian Journal of Remote Sensing and Space Science,* 24**,** 119-130.

MOHAMED, S. A. 2019. Application of satellite image processing and GIS-Spatial modeling for mapping urban areas prone to flash floods in Qena governorate, Egypt. *Journal of African Earth Sciences,* 158**,** 103507.

MUSTAFA, A. M., MUHAMMED, H. & SZYDŁOWSKI, M. 2019. Extreme rainfalls as a cause of urban flash floods; a case study of the Erbil-Kurdistan region of Iraq. *Acta Scientiarum Polonorum Formatio Circumiectus,* 18**,** 113-132.

NOTARO, V., FONTANAZZA, C. M., FRENI, G. & PULEO, V. 2013. Impact of rainfall data resolution in time and space on the urban flooding evaluation. *Water science and technology,* 68**,** 1984-1993.

OUBENNACEUR, K., CHOKMANI, K., NASTEV, M., LHISSOU, R. & EL ALEM, A. 2019. Flood risk mapping for direct damage to residential buildings in Quebec, Canada. *International journal of disaster risk reduction,* 33**,** 44-54.

PORTUGUÉS-MOLLÁ, I., BONACHE-FELICI, X., MATEU-BELLÉS, J. & MARCO-SEGURA, J. 2016. A GIS-Based Model for the analysis of an urban flash flood and its hydro-geomorphic response. The Valencia event of 1957. *Journal of Hydrology,* 541**,** 582-596.

RAHMANI, V., HUTCHINSON, S. L., HARRINGTON JR, J. A. & HUTCHINSON, J. S. 2016. Analysis of frequency and magnitude of extreme rainfall events with potential impacts on flooding: A case study from the central United States. *International Journal of Climatology,* 36**,** 3578-3587.

ROSSMAN, L. A. 2010. *Storm water management model user's manual, version 5.0,* National Risk

Management Research Laboratory, Office of Research and ….

SAMELA, C., ALBANO, R., SOLE, A. & MANFREDA, S. 2018. A GIS tool for cost-effective delineation of flood-prone areas. *Computers, Environment and Urban Systems,* 70**,** 43-52.

SILLANPÄÄ, N. & KOIVUSALO, H. 2015. Impacts of urban development on runoff event characteristics and unit hydrographs across warm and cold seasons in high latitudes. *Journal of Hydrology,* 521**,** 328-340.

TENG, J., JAKEMAN, A. J., VAZE, J., CROKE, B. F., DUTTA, D. & KIM, S. 2017. Flood inundation modelling: A review of methods, recent advances and uncertainty analysis. *Environmental modelling & software,* 90**,** 201-216.